

# An Effective Control Approach of Hybrid Energy Storage System Based on FLC/Grey Wolf Optimisation

V. Prasanna\* and G. Ravi

## ABSTRACT

In the modern era, the integration of renewable energy sources (RES) has bolstered the autonomy of urban energy infrastructures, reducing reliance on distant sources and grids. Batteries serve as a vital bridge between power supply and fluctuating load demands within RES systems. However, the unpredictable nature of RES behavior and varying load requirements often subject batteries to repeated deep cycles and irregular charging patterns. These cycles diminish the battery's lifespan and escalate replacement costs. This study presents an innovative control strategy for a Solar-Wind model featuring a Battery-Supercapacitor Hybrid Energy Storage System. The objective is to prolong the battery's operational lifespan by mitigating intermittent strain and high current demands. In contrast to conventional methods, the proposed control approach incorporates a Low-Pass Filter (LPF) and a Fuzzy Logic Controller (FLC). Firstly, the LPF minimizes the oscillations in battery consumption. Simultaneously, the FLC optimizes the high current demand on the battery while vigilantly monitoring the supercapacitor's charge levels. Moreover, Grey Wolf Optimization (GWO) is employed to fine-tune the FLC's membership functions, ensuring optimal peak current attenuation in batteries. The effectiveness of the proposed model is benchmarked against standard control techniques, namely Rule-Based Controller and Filtration-Based Controller. Comparative analysis reveals that the proposed method substantially reduces peak current and high power requirements of the battery. Consequently, this enhances the utilization of the supercapacitor, significantly augmenting the battery's operational life. The results demonstrate a remarkable improvement over conventional systems, emphasizing the potential of this approach in optimizing energy storage systems for sustainable, long-term performance.

Submitted: January 10, 2024

Published: April 01, 2024

 10.24018/ejeng.2024.9.2.3113

Puducherry Technological University,  
India.

\*Corresponding Author:  
e-mail: text2prasanna@gmail.com

**Keywords:** Energy storage system, Grey wolf optimization algorithm, PV-wind system, REPS.

## 1. INTRODUCTION

In Renewable Energy Systems (RES), batteries play a crucial role in bridging the power gap between supply and varying load demands. However, due to the unpredictable nature of RES and the fluctuating power requirements of loads, batteries often undergo frequent deep cycles and irregular charging patterns, leading to a shortened lifespan and increased replacement costs [1]–[3]. To mitigate these challenges, Hybrid Energy Storage Systems (HESS) have emerged as a viable solution, reducing battery strain, capacity, and overall system costs [4].

Managing the power dynamics of both batteries and supercapacitors (SC) is essential to maximize energy consumption and conservation in the Battery-SC model. Aiming to increase battery lifespan by reducing peak current needs and constant stress is a common objective in HESS deployment [4], [5]. By minimizing peak current, voltage drop is lessened, enhancing battery efficiency and reducing overheating and dynamic stress [5], [6].

While fuzzy logic controllers (FLC) are widely used in Battery-Hydrogen Storage Systems (HSS), their application in RES with Battery-SC Systems is relatively unexplored. FLC, known for its simplicity and insensitivity to system changes, minimizes battery capacity

loss significantly when compared to battery-only systems [7]. However, the challenge lies in optimizing FLC's membership functions (MFs), traditionally done through time-consuming trial-and-error methods [8].

In this research, a novel control model for a PV-Wind power system with Battery-SC is proposed. The control approach aims to reduce the battery's fluctuating active strain and high current demands while ensuring optimal state of charge for the supercapacitor (SOC<sub>sc</sub>) [8]. Employing a Sugeno-type FLC, known for its efficiency and robustness, the model adjusts the power flow between the battery and SC based on real-time power needs and SOC<sub>sc</sub>. To enhance FLC's performance, the Grey Wolf Optimization (GWO) algorithm is employed, optimizing the FLC's membership functions to decrease high battery current.

Simulink is utilized to compare the proposed system's performance against traditional systems, using a rural household load profile. The results showcase the efficiency of the proposed control model, demonstrating its potential in significantly improving the performance and lifespan of Battery-SC systems. This paper presents the Simulink models of the suggested system, highlights the GWO optimization results, and compares the outcomes with conventional systems, shedding light on the promising future of optimized Battery-SC RES applications.

## 2. SYSTEM MODELLING AND COMPONENTS

A solar panel, a wind turbine, and a battery (lithium-ion) are all part of the proposed hybrid system, which also includes an SC. As indicated, all of the elements are coupled to a voltage unified DC bus [9].

### 2.1. Wind Turbine Modelling

In this study, we'll use a wind turbine powered by a permanent synchronous generator (PMSG). The wind turbine's power and rated wind velocity are 300 W and 13 m/s, respectively. The maximum wind velocity is 18 m/s, with a beginning wind velocity of 3 m/s. The maximal power production is 800 W [10].

The output power of a wind turbine can be stated as follows using aerodynamic theory:

$$P = 0.5\rho\pi R^2V^2C_{mp}(\lambda, \beta) \quad (1)$$

where  $P$  is the resultant power of a wind turbine generator. The air density, wind speed and blade radius are represented by,  $R$ , and  $V_w$ , discretely. The power coefficient ( $C_p$ ) is defined as:

$$C_p(\lambda, \beta) = 0.73(151/\lambda - 0.58\beta - 0.002\beta^{2.14} - 13.2)e^{-18.4/\lambda} \quad (2)$$

where:

$$\lambda = \frac{1}{1/((\lambda - 0.02\beta) - (0.003/\beta^3 + 1))} \quad (3)$$

In Matlab, a fluctuating wind of 13 m/s is generated and shown. The wind turbine's output power under MPPT control is displayed [11].

### 2.2. PV Array Modelling

A solar array is formed by connecting numerous parallel and series solar cells. The following equation is used to compute the short-circuit current for every solar cell [11]:

$$I_{SC} = I_{SC0}(G/G_0)a \quad (4)$$

where  $I_{sc}$  and  $I_{sc0}$  are the short-circuit currents,  $G$  and  $G_0$  are standard solar radiation, respectively.

The PV cell's open-circuit voltage is:

$$V_{oc} = \frac{V_{oc0}}{1 + \beta \ln \frac{G}{G_0}} \left( \frac{T_0}{T} \right)^\alpha \quad (5)$$

where  $V_{oc}$  and  $V_{oc0}$  are the open-circuit voltages under average and normal solar energy  $G$  and  $G_0$ , respectively, and  $T$  is the PV cell temperature.  $\beta$  is a technology-specific coefficient for PV cells that depicts temperature nonlinear effects. Using cells arranged in series ( $N_s$ ) and cells arranged in parallel ( $N_p$ ), the highest power from the solar array can be written as [12]:

$$P_{max} = N_p N_s \frac{(V_{oc0}/nkTq) - \ln((V_{oc}/nkTq) + 0.72)}{1 + (V_{oc0}/nkTq)} \times \frac{1 - R_s}{V_{oc}/I_{sc}} V_{oc} I_{sc} \quad (6)$$

Because both the wind turbine and the solar array create power, the collective power produced may be estimated by summing them together. Furthermore, we presume a constant load need of 1 kW. As a result, the power disparity between produced and needed power by load is  $P$  [13].

$$\Delta P = P_{WP} + P_{PV} - P_L \quad (7)$$

where  $P_{WP}$ ,  $P_{PV}$ , and  $P_L$  are the power output of a wind turbine, power of the solar array, and power demand of the load, discretely [14].

### 2.3. Battery-SC Storage System

An SC, a bidirectional DC-DC converter, control circuitry, and a battery bank are all included in the proposed system's HESS, as shown in the Simulation of the solar-wind system with Battery-SC system [15]. The Simulink library contains the structure and details of the Battery and Supercapacitor models. The Battery-SC system described in this work uses the benefits of both high power density and energy density storage to accomplish the necessary performance [16]. However, combining the battery-SC as a solitary source of power necessitates a sophisticated conditioning circuitry [17]. Because the SC voltage varies greatly because of its low energy density, the proposed Model's Battery-SC system is built in a partially active architecture, with a bi-directional DCDC converter located adjacent to the Supercapacitor to isolate the Supercapacitor from the rest of the system [18].

The power electronic component is made up of a DC-DC converter and control circuits [19]. This design provides enough flexibility to implement a variety of control techniques as shown in Fig. 1. Furthermore, with the employment of a single DC-DC converter, this design provides a favourable trade-off between functionality and

TABLE I: PROPOSED SYSTEM'S SPECIFICATIONS

Component	Rating	Value
PV	Power	1.2 kW
Wind system	Power	300 W
Li ion battery	Voltage	48 V
	Capacity	300 Ah
Supercapacitor	Voltage	45 V
	Capacitance	500 F

intricacy of the circuit [20]. It is also necessary to manage the power flow in both directions to properly link the batteries and SCs. The System's specifications are shown in Table I.

The bidirectional half-bridge DC-DC converter can operate in both buck and boost modes. It comprises of two bi-positional switches constructed in a half bridge arrangement using transistors S1/S2 and diodes D1/D2 [21]. The converter's high and low voltage sides are interfaced to the DC bus and the Supercapacitor, to enable for constant functioning of the SC [22]. Power is transmitted from the high to the low voltage side when the converter is in buck mode (inductor current,  $i_L > 0$ ). Power is transmitted from the low to the high voltage side ( $i_L < 0$ ) while the converter is in boost mode. The following is a description of the proposed system's dynamic power balance, based on Fig. 2:

$$P_{PV} + P_{batt} + P'_{SC} + P_{Load} = 0 \quad (8)$$

where  $P_{PV}$  is the PV's power generation,  $P_{batt}$  is the battery's power,  $P_{load}$  is the load's power demand, and  $P_{sc0}$  is the SC power flow after the DC-DC converter's power conversion. The converter's efficiency is less than 100% in real-world operation.

As a result, the power shift from the SC to the DC bus is written as expression (9):

$$P'_{SC} = \eta_{DCDC} \times P_{SC} \quad (9)$$

where  $P_{SC}$  denotes SC's power flow and  $\eta_{dc}$  denotes the converter's efficiency. The converter's efficiency is presumed to be 100% in the context of this research.

As a result, (10) defines the amount of power needed by the Battery-SC,  $\Delta P$ , which is the difference between  $P_{PV}$  and  $P_{load}$ 's output power:

$$\Delta P = P_{PV} - P_{Load} = P_{batt} + P_{SC} \quad (10)$$

### 3. CONTROL STRATEGY

The control strategy, which is based on current system conditions, controls the HESS power flow. In order to accomplish various objectives is frequently complicated and calls for constant operation. Optimizing HESS control is essential for maximizing sustainability and energy efficiency [23]–[28].

There are two different categories of control strategies: traditional control techniques and modern control techniques [29]. Rule-based controllers (RBC) and filtering-based controllers (FBC) are examples of traditional control systems that are simple and easy to implement since they don't need intensive processing. However, they tend to be rigid and sensitive to parameter changes [30]. Because they develop the dynamic behavior without needing an accurate description of the system, modern control techniques like the FLC are more dependable and effective than traditional control strategies [31]. The MFs of FLC, on the other hand, are normally calculated through trial-and-error, which is ineffective and a lengthy process.

To summarize, REPS with Battery-Supercapacitor HESS frequently use traditional control mechanisms like RBC and FBC. In this study, the proposed control approach is compared to two common traditional control systems (RBC and FBC). All models with SC have a SOCsc operating range of 50% to 100% to enable the use of 75% of the total SC energy [32].

#### 3.1. Rule-Based Controller

Based on a set of guidelines, the RBC determines how much power is distributed between the SC and battery. It is easy to implement because it does not necessitate complex processing. RBC, on the other hand, is extremely sensitive to parameter variations due to its pre-defined rules and

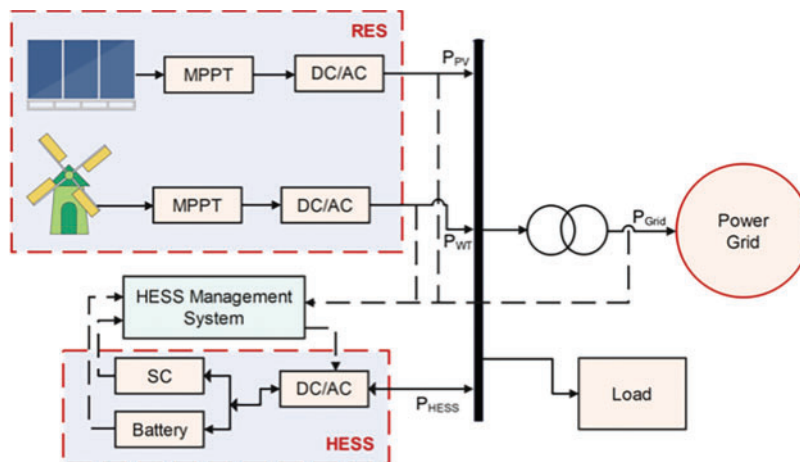


Fig. 1. Hybrid energy storage and renewable energy system.

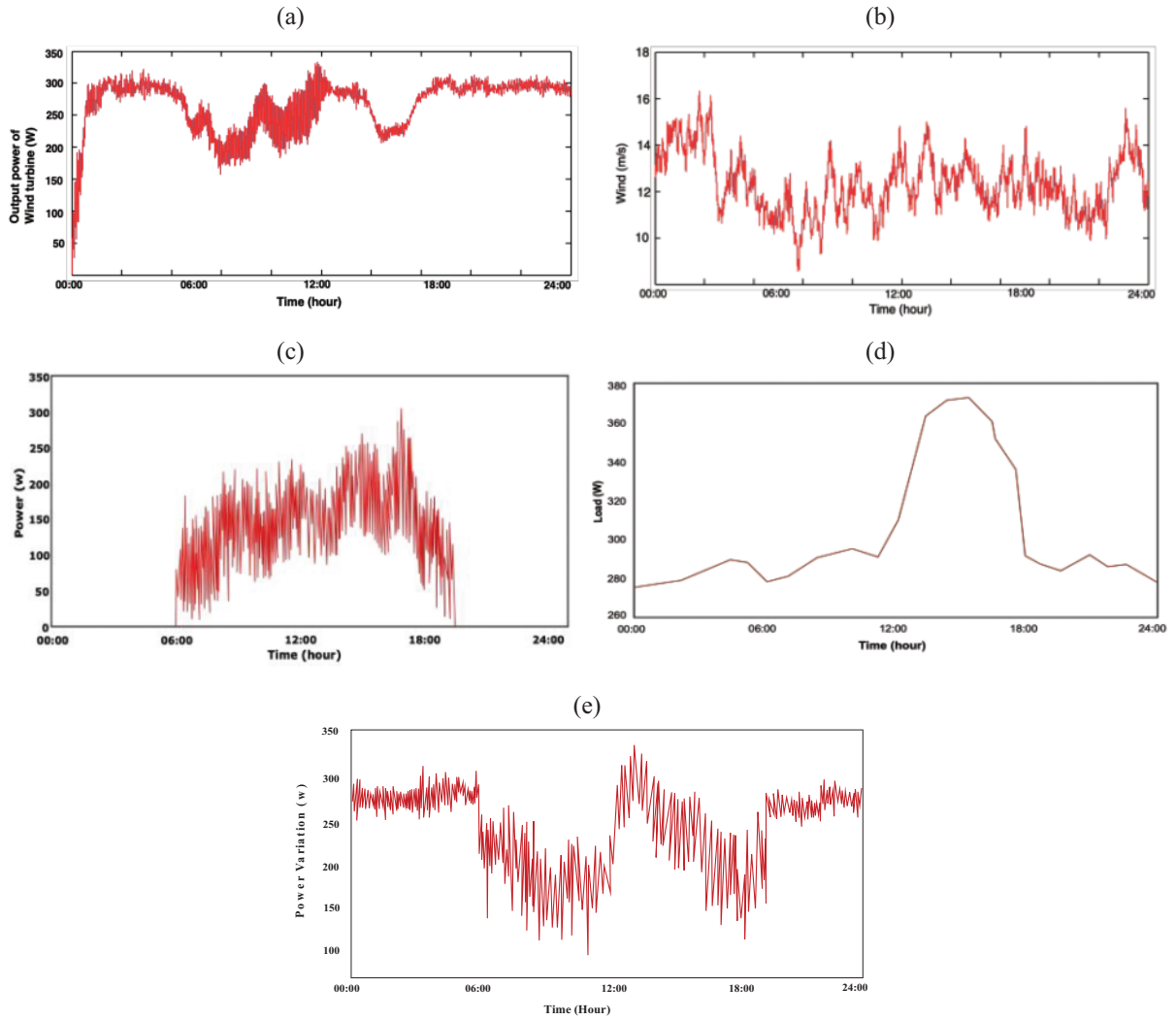


Fig. 2. Simulation inputs: (a) Solar power output, (b) Wind speed, (c) Output from wind turbine, (d) Load profile, (e) Power variation between Power generation and Load demand.

procedures. An RBC is created and depicted as a dead-zone function using data from [33]. Whenever the current of the battery is between the  $ib1$  and  $ib2$  thresholds, the battery is the sole way to supply the load requirement. when the  $ib1$  or  $ib2$  threshold is reached for battery current demand, the extra current demand is divided between the SC and the battery according to the  $K1$  or  $K2$  ratio [33].

### 3.2. Filtration Based Controller

The FBC splits the active elements of the power demand into low-frequency and high-frequency parts using a filter. This method is easy and requires little computing power. A high pass filter (HPF)-based FBC's structure was borrowed from [34]. The HPF divides the power requirement into high-frequency (PHF) and low-frequency (PLF) components, with the PHF and PLF fetched by the battery and SC, discretely.

### 3.3. Proposed Control Strategy

Fig. 3 depicts the framework of the suggested control method, which attempts to reduce the battery's active tension and high current demand. The energy management device in the control strategy is a fuzzy logic controller (FLC). The Grey Wolf Optimization optimisation (GWO)

technique is used to optimise the FLC's membership functions (MFs) in order to obtain optimal performance. The next sections discuss the structure of the suggested control strategy.

### 3.4. DC Bus Configuration and Optimization

The voltage on the DC bus is managed using the principle expressed in Fig. 3. The PI device decides the reference current of the DC bus  $I_{dc_{ref}}$  to regulate the bus voltage at  $V_{ref} = 400$  V.

The EMS generates the reference currents for batteries and SCs ( $I_{bat_{ref}}$  and  $I_{sc_{ref}}$ , correspondingly). These reference currents makes the DC bus voltage to remain static irrespective of load conduct or fluctuations in power output. When a fault develops on an element such as SOC, power interruption, or solar irradiation variation, the batteries and/or SCs make sure that the DC bus voltage is regulated. The collective reference currents,  $I_{sc_{ref}}$  and  $I_{bat_{ref}}$ , should be same as  $I_{dc_{ref}}$  at all times:

$$I_{dc_{ref}} = I_{sc_{ref}} + I_{bat_{ref}} \quad (11)$$

The following equation can be used to simulate the function of a DC bus:

$$C_{dc} dv_{dc}/dt = I_{sc_{dc}} + I_{bat_{dv}} - I_{load} \quad (12)$$



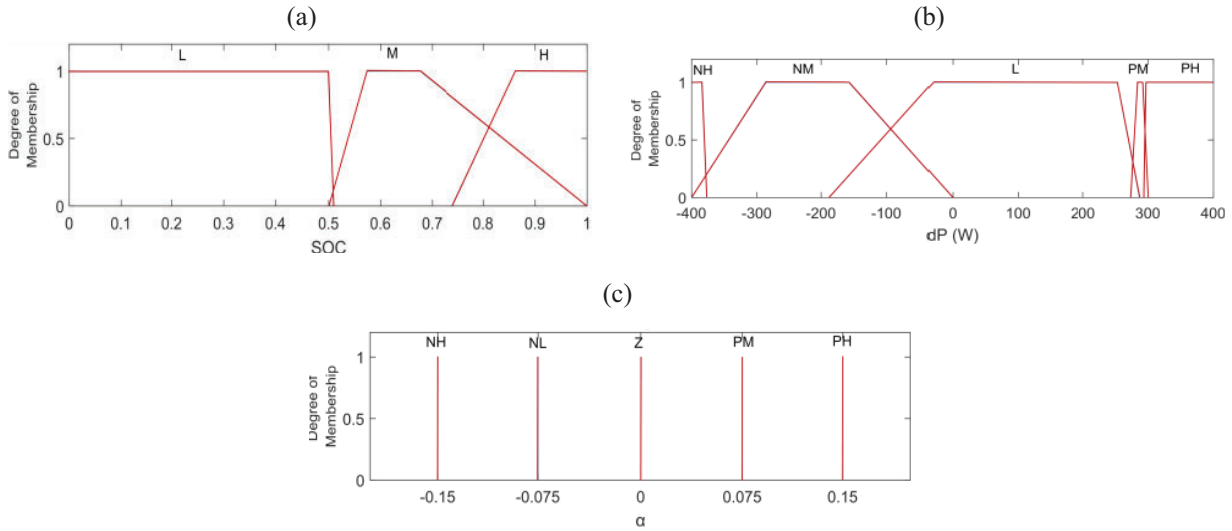


Fig. 4. Membership functions: (a) Input 1:  $P_{LF}$ , (b) Input 2:  $SOC_{sc}$ , (c) Output:  $\alpha$ .

TABLE II: RULES OF FLC

		$\Delta P$				
		PH	PL	L	NL	NH
$SOC_{sc}$	H	PH	PL	Z	Z	Z
	M	PL	PL	Z	NL	NL
	L	Z	Z	Z	NL	NH

### 3.7. Grey Wolf Optimization (GWO) Algorithm

The Grey Wolf Optimization approach is based on the transverse orientation mobility of ants in environment. While exploring their environment, real ants leave pheromone trails that direct each other to resources. Similarly, the simulated ants record their positions and the quality of their solutions in the same way so that more ants find better solutions in subsequent simulation iterations. Therefore, during each flight, Ants function as particles that change their positions and velocities based on their own  $A_{best}$  as well as the collective group's  $G_{best}$  experience (iteration).

The amount of variables within every problem decides the size of the particles. A fitness function calculated at

the particle's current position determines the quality of the solution for each particle.

The FLC may be optimised based on the projected data since the electrical load, and RES can both be forecasted. In this investigation, the load demand and RES profile presented in Figs. 2d and 2e are taken as the baseline model. The anticipated RES data and load demand are used to optimise the MFs of the FLC's input variables. Four points together form a complete trapezoidal MF. The first (left) MF and the last (right) MF of a variable with more than two trapezoidal MFs each have just two tuning points. As a result, the equation can be used to determine the number of points that are optimal for a given variable,  $n$  (18):

$$n = (4 \times mf) - 4 \tag{18}$$

where  $mf$  is the number of MF, in this case. PLF and  $SOC_{sc}$ , two input variables, have five and three MFs, respectively, in the suggested control approach. Because of this, the GWO algorithm must optimise 24 points altogether. In light of this, A 24-dimensional particle can be used to represent an FLC or solution. The population size and the number of iterations are user-defined in the GWO procedure, as shown in Fig. 6.

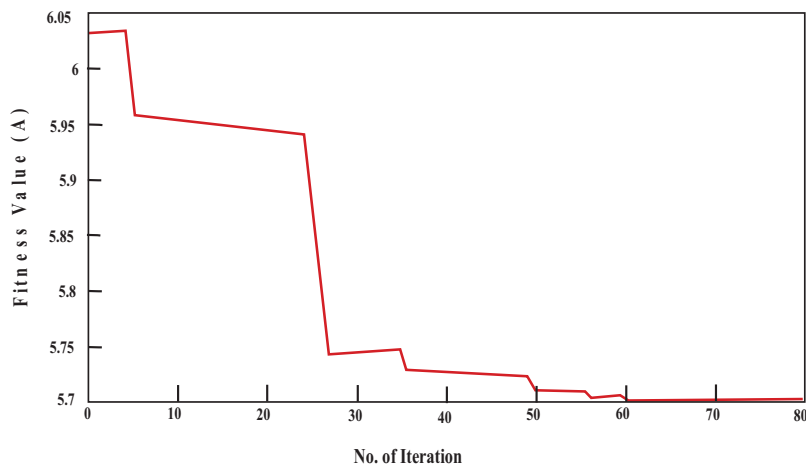


Fig. 5. GWO algorithm's convergence curve after 80 iterations of optimization.

TABLE III: MODEL CONFIGURATIONS

Model	Energy source	Energy storage system	Control strategy
I	PV/Wind	Battery/SC	RBC
II	PV/Wind	Battery/SC	FBC
III	PV/Wind	Battery/SC	FLC/GWO (Proposed control strategy)

3.8. Fitness Function

The battery’s high discharge current causes extreme damage since it raises the battery’s temperature and the pace at which positive active mass sludges. The major goal is to reduce the battery high current while keeping the SC above 50% of SOCsc. The system’s cost can be decreased while also increasing battery efficiency and lifespan due to the reduction in battery peak current [35]–[37]. The fitness function,  $f$ , evaluates the solution’s fitness in GWO. In this study, the minimum battery current, denoted by  $f(x)$ , is defined in (19):

$$f(x) = \min(I_{batt}) \tag{19}$$

where  $I_{batt}$  stands for the battery current. The highest battery current of every function is noted for the GWO algorithm to find the best one in each iteration.

4. RESULTS AND DISCUSSION

4.1. GWO Algorithm

Based on the load profiles depicted in Fig. 2, GWO optimises the MFs of FLC. The flowchart for GWO optimization is shown in Fig. 6, where a population size of 20 ants and a total of 80 iterations are specified. Each 24-dimensional particle represents an FLC model. Everywoflin, the population is regulated using the fitness function, which is described in (19). After each evaluation, the ant’s individual best ( $A_{best}$ ) and overall best ( $G_{best}$ ) are updated.

The fitness value versus iteration count graph is shown in Fig 5. Using a randomly generated solution, the first iteration’s  $G_{best}$  is 6.0389 A. As iterations go longer, the fitness value gets lower. The  $G_{best}$  is maintained at 5.718 A through the 80<sup>th</sup> iteration after being decreased to that value at the 60<sup>th</sup> iteration. By the time the optimization procedure is complete, the top choice (the particle with  $G_{best}$  of 5.718 A) has been converted into an FLC model, as shown in Fig. 4.

4.2. Simulation

Simulink is used in this study to build the three models stated in the Table III. The solar-wind system with battery-SC model and RBC is referred as Model I. The Solar-wind system with battery-SC model and HPF-based FBC is named as Model II. The hybrid PV-wind system with battery-SC model and the suggested control approach makes up Model III. Table III depicts the configuration of the control strategies. The power source and load profiles are modelled and adapted to all models, as shown in Fig. 2.

A number of battery metrics are assessed, including average battery SOC ( $SOC_{batt\ average}$ ), peak battery current

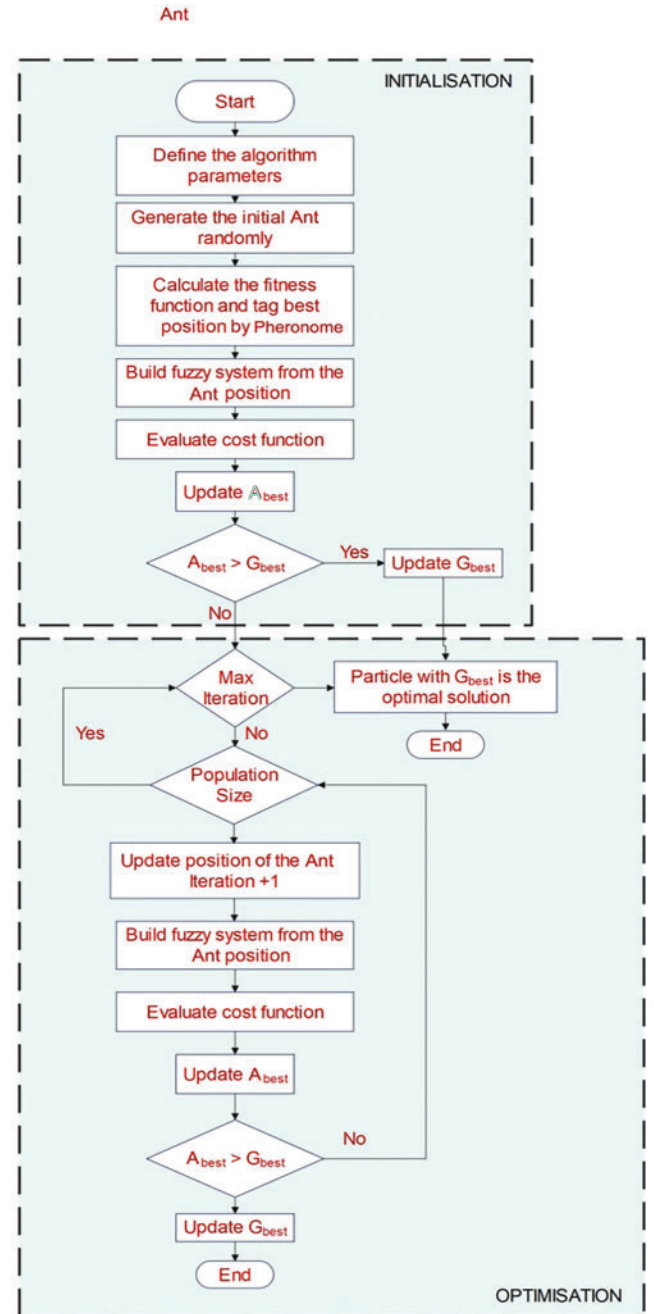


Fig. 6. Flowchart of GWO process.

( $I_{batt\ peak}$ ), peak battery power ( $P_{batt\ peak}$ ), and final battery SOC ( $SOC_{batt\ final}$ ). Lower battery stress, greater battery efficiency, and a decrease in internal voltage are all effects of reducing  $I_{batt\ peak}$  and  $P_{batt\ peak}$  [4], [5]. In this study, the  $SOC_{batt\ average}$  and  $SOC_{batt\ final}$  are examined. Higher  $SOC_{batt\ average}$  and  $SOC_{batt\ final}$  would increase the life of battery and decrease system LPSP.

$|\Delta P|$  stands for the absolute rate of change of power in a time step of  $dt$ , expressed in Watt per second (W s1). Equation (20) can be utilised to calculate  $|\Delta P|$ :

$$|\Delta P| = |(P(t) - P(t - \Delta t)) / \Delta t| \tag{20}$$

where  $P(t)$  denotes battery power at time  $t$ ,  $P(t - \Delta t)$  denotes battery power at time  $t - \Delta t$ , and  $\Delta t$  is the study’s 1 s time step. In other words,  $|\Delta P|$  can be used to estimate the battery power’s amount of fluctuation, with a greater

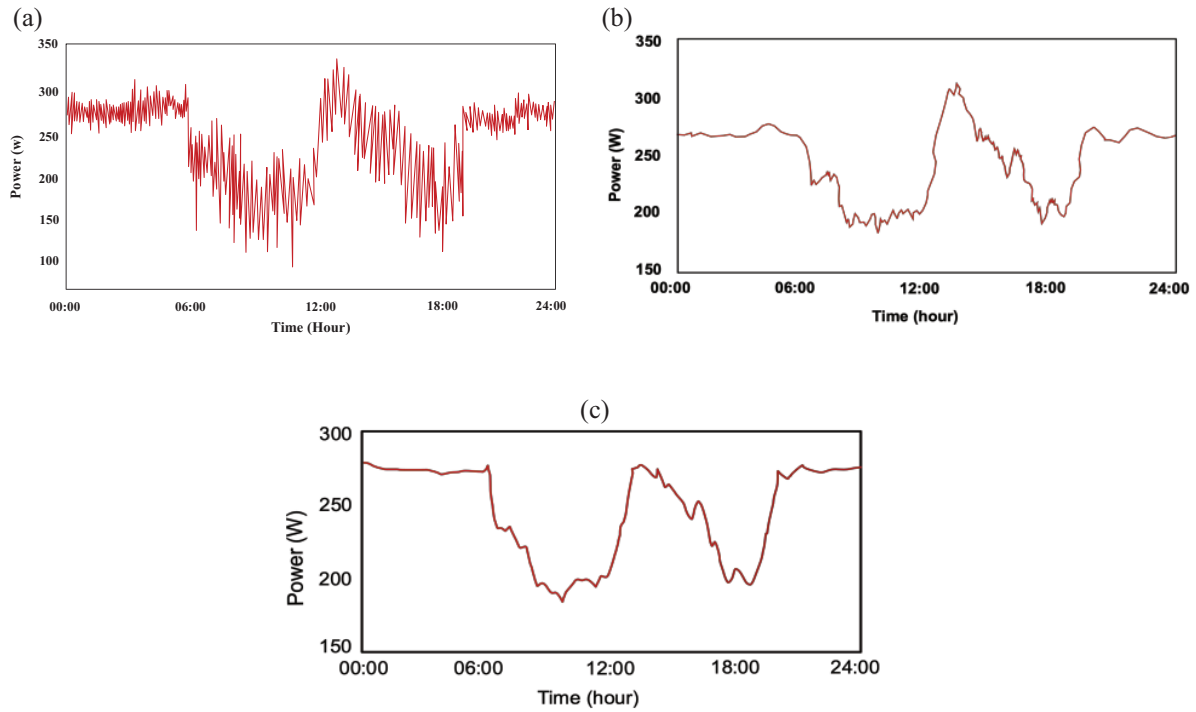


Fig. 7. Battery power (a) Battery power—Model I, (b) Battery power—Model II, (c) Battery power—Model III.

TABLE IV: SUMMARY OF BATTERY PERFORMANCE

Battery parameters	Value	Model I	Model II	Model III
$I_{batt\_peak}$	Current (A)	6.053	6.152	5.718
	Attenuation (%)	–	–1.02	5.9
$P_{batt\_peak}$	Power (W)	293.6450	296.5788	275.4768
	Attenuation (%)	–	–1.01	6.19
$SOC_{batt\_average}$	SOC (%)	67.3008	66.7895	67.2767
	Increase (%)	–	0.76	0.4
$SOC_{batt\_final}$	SOC (%)	47.8976	47.7657	47.8734
	Increase (%)	–	0.01	1.15
$ \Delta P _{max}$	Rate (ws-1)	24.1243	8.7685	7.4899
	Attenuation (%)	–	74.17	77.01
$ \Delta P _{mean}$	Rate (ws-1)	0.346	0.017869	0.01567
	Attenuation (%)	–	95.01	95.59

value indicating a higher level of variation. Low levels of battery power fluctuation can boost the battery’s efficiency and life expectancy.

This study computes the battery power’s maximum  $|\Delta P|$   $|\Delta P_{max}|$  and mean  $|\Delta P|$   $|\Delta P_{mean}|$  to assess the battery’s level of dynamic stress.

The simulation model of all battery profiles simulation are shown in Figs. 7a–7c. Table IV compares and summarises each model’s battery performance.

The  $I_{batt\_peak}$  and  $P_{batt\_peak}$  are decreased for Model II, according to Fig. 7b and Table IV, but the battery still endures a significantly variable power demand. As the SC expends most of its energy to deliver the load, the  $SOC_{batt\_average}$  and  $SOC_{batt\_final}$  are increased by 0.76 percent and 0.01 percent, discretely. These improvements are the largest of all the models. Table IV and Fig. 7b for Model II demonstrate a notable decrease in the active strain of the battery but only a marginal improvement in  $I_{batt\_peak}$  and  $P_{batt\_peak}$ . This is due to the FBC, which was created to lessen the dynamic load on the battery

without taking peak demand into account. However, the  $SOC_{batt\_average}$  and  $SOC_{batt\_final}$  are not significantly developed (0%), as the SC only absorbs the highly fluctuating low power components.

As shown in Fig. 7, the battery power profile for Model III is noticeably smoother than that of Models I and II. SC compensates for the difference between  $\Delta P$  and battery power.

As previously stated, one of the suggested model’s objectives is to attenuate the battery’s peak demand. The maximum battery current in Model III in the simulation is 5.718 A, which is identical to the best because the GWO optimization and simulation use the same energy source and load profiles.

Due to the FLC’s inclusion in the suggested control plan, the SC delivers to satisfy the high demand while continuously taking its SOC level into account. As a result, when compared to Model I, the  $I_{batt\_peak}$  and  $P_{batt\_peak}$  are decreased by 5.9% and 6.19%, discretely.

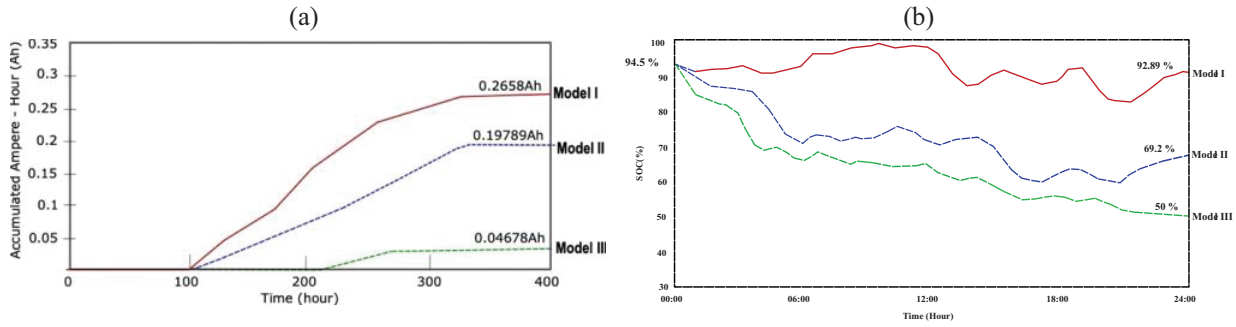


Fig. 8. Supercapacitor rating: (a) Accumulated ampere hour of supercapacitor, (b) State of charge of capacitor.

Since the SC expends the majority of its energy achieving the control strategy's objectives, the  $SOC_{batt\ average}$  and  $SOC_{batt\ final}$  are enhanced by 0.4% and 1.15%, discretely which is significantly less than Model I.

By determining the absolute value of the total ampere-hours (amount of charge) travelling to and from the SC,  $|Ah|_{SC}$ , it is possible to estimate the SC utilisation in the HESS. The SC current is integrated over time to determine the SC ampere-hours.

The  $SOC_{sc}$  and  $|Ah|_{SC}$  of Models I, II, and III are shown in Fig. 8 during the simulation. The level of battery use decreases as SC utilisation increases. As a result, by raising the SC utilisation level, the system's internal losses can be decreased. By boosting SC use, the system can be made smaller. This is because a significant portion of the resultant current passes via the SC, which has a lower internal resistance and, as a result, causes the battery to heat up less and last longer.

According to Fig. 8b, Model I's final  $SOC_{sc}$  is same as the required minimum  $SOC_{sc}$  of 50%. On comparison, Model I performs the poorest in terms of SC utilisation and battery active strain reduction, meaning that it does not properly use the SC. It also consumes the majority of the SC energy. The result is that Model II's total  $|Ah|_{SC}$  is 32.65% less than Model III but 487.86% more than Model I. Only 0.56% net  $SOC_{sc}$  is used during the simulation, resulting in a final  $SOC_{sc}$  of Model II of 92.69%.

In other words, Model II's SC is not fully utilised. In Model III, the final  $SOC_{sc}$  is kept at a greater level than in Model I while being kept 7.45% over the required minimum SOC of 50%. In compared to the other models, Model III has the greatest total  $|Ah|_{SC}$ , with Model I and Model II's respective SC utilisation levels being 687.122% and 32.65% lower.

In other words, the suggested technique can run the SC under the specified SOC range and effectively utilise the SC's constricted energy limit to produce promising performance.

The suggested system (Model III) is tested using the load profile depicted in Fig. 2b and various weather conditions. As would be expected, the scenario's most important changes are the decrease in Peak demand and strain level of the battery.

Regardless of the weather and load profile, the simulation results demonstrate that the suggested method greatly attenuates the battery's active strain  $\Delta P_{mean}$  by more than 80% when compared to Model I. In the meantime, the decrease in battery's high need depends on the stress level

of  $\Delta P$ , which is established by the power source and the load demand. With the high  $\Delta P$  and low PV output or peak load demand, the battery peak demand can be significantly reduced [38].

## 5. CONCLUSION

In conclusion, this research underscores the pivotal role of innovative control strategies in enhancing the longevity and efficiency of energy storage systems, particularly in the context of modern urban energy infrastructures reliant on renewable sources. By addressing the challenges posed by the unpredictable behaviour of renewable energy sources and varying load demands, the study presents a significant step forward in sustainable energy solutions.

The proposed control approach, integrating a Low-Pass Filter (LPF), Fuzzy Logic Controller (FLC), and Grey Wolf Optimization (GWO), stands out as a pioneering method to tackle the detrimental effects of deep cycles and irregular charging patterns on batteries. Through the meticulous optimization of FLC's membership functions using GWO, the system achieves optimal peak current attenuation, reducing the strain on batteries substantially. The simultaneous monitoring and adjustment of the supercapacitor's charge levels further contribute to maximizing the operational life of the entire hybrid energy storage system.

Comparative analyses against traditional control techniques, such as Rule-Based Controller and Filtration-Based Controller, demonstrate the superiority of the proposed method. Substantial reductions in peak current and high power requirements not only alleviate strain on the battery but also significantly enhance the utilization of the supercapacitor. This improvement not only augments the system's efficiency but also mitigates replacement costs, contributing to the long-term sustainability of energy storage solutions.

In essence, this study exemplifies the potential of integrating advanced control methodologies and optimization techniques in shaping the future of energy storage systems. By extending the operational life of batteries, this research paves the way for more reliable, cost-effective, and environmentally friendly energy infrastructures, fostering a greener and more sustainable future.

## REFERENCES

- [1] Jakhriani AQ, Othman A-K, Rigit ARH, Samo SR. Life cycle cost analysis of a standalone PV system. *2012 Int. Conf. Green Ubiquitous Technol*, pp. 82–85, Jakarta, Indonesia: Green Ubiquitous Technol, IEEE; 2012. 10.1109/GUT.2012.6344195.
- [2] Kan SY, Verwaal M, Broekhuizen H. The use of battery-capacitor combinations in photovoltaic powered products. *J Power Sourc.* 2006;162:971–74. doi: 10.1016/j.jpowsour.2005.07.001.
- [3] Schiffer J, Sauer DU, Bindner H, Cronin T, Lundsager P, Kaiser R. Model prediction for ranking lead-acid batteries according to expected lifetime in renewable energy systems and autonomous power-supply systems. *J Power Sourc.* 2007;168:66–78. doi: 10.1016/j.jpowsour.2006.11.092.
- [4] Baisden AC, Emadi A. ADVISOR-based model of a battery and an ultra-capacitor energy source for hybrid electric vehicles. *IEEE Trans Veh Technol.* 2004;53:199–205. doi: 10.1109/TVT.2003.822004.
- [5] DouGWOL RA, Liu S, White RE. Power and life extension of battery-ultracapacitor hybrids. *IEEE Trans Components Packag Technol.* 2002;25:120–31. doi: 10.1109/6144.991184.
- [6] Pay S, Baghzouz Y. Effectiveness of battery-supercapacitor combination in electric vehicles. *2003 IEEE Bol. PowerTech—Conf. Proc.*, pp. 728–33, 2003. doi: 10.1109/PTC.2003.1304472.
- [7] Song Z, Hofmann H, Li J, Hou J, Han X, Ouyang M. Energy management strategies comparison for electric vehicles with hybrid energy storage system. *Appl Energ.* 2014;134:321–31. doi: 10.1016/j.apenergy.2014.08.035.
- [8] Altin N, Sefa I. dSPACE based adaptive neuro-fuzzy controller of grid inter-active inverter. *Energy Convers Manag.* 2012;56:130–39. doi: 10.1016/j.enconman.2011.11.017.
- [9] Azar AT. *Fuzzy Systems*. 1st ed. Vukovar, Croatia: InTech; 2010. doi: 10.5772/56527.
- [10] Mellit A, Pavan AM. A 24-h forecast of solar irradiance using artificial neural network: application for performance prediction of a grid-connected PV plant at Trieste, Italy. *Sol Energ.* 2010;84:807–21. doi: 10.1016/j.solener.2010.02.006.
- [11] Mghouchi YEL, Ajzoul T, Bouardi AEL. Prediction of daily solar radiation intensity by day of the year in twenty-four cities of Morocco. *Renew Sustain Energy Rev.* 2016;53:823–31. doi: 10.1016/j.rser.2015.09.059.
- [12] Mghouchi YEL, Ajzoul T, Taoukil D, El Bouardi A. The most suitable prediction model of the solar intensity, on horizontal plane, at various weather conditions in a specified location in Morocco. *Renew Sustain Energy Rev.* 2016;54:84–98. doi: 10.1016/j.rser.2015.09.089.
- [13] Lee K, Cha Y, Park J. Short-term load forecasting using an artificial neural network. *Power Syst IEEE Trans.* 1992;7:124–132. Available from: [http://ieeexplore.ieee.org/xpls/abs\\_all.jsp?arnumber=14141695](http://ieeexplore.ieee.org/xpls/abs_all.jsp?arnumber=14141695).
- [14] Banda E, Folly K. Short-Term load forecasting using artificial neural network techniques load forecasting using artificial neural network. *Conference: Power Tech, IEEE Lausanne*, 2009. doi: 10.1109/PCT.2007.4538301.
- [15] Park DC, El-Sharkawi MA, Marks RJ, Atlas LE, Damborg MJ. Electric load forecasting using an artificial neural network. *IEEE Trans Power Syst.* 1991;6:442–9. doi: 10.1109/59.76685.
- [16] MathWorks I. Comparison of Sugeno and Mamdani systems. 2016. Available from: <http://www.mathworks.com/help/fuzzy/comparison-of-sugeno-and-mamdani-systems.html> (accessed April 3, 2016).
- [17] Song YD, Cao Q, Du X, Karimi HR. Control strategy based on wavelet transform and neural network for hybrid power system. *J Appl Math.* 2013;2013:1–8. doi: 10.1155/2013/375840.
- [18] Pecun R, Nayir A. Design and implementation of a 12 kW wind-solar distributed power and instrumentation system as an educational testbed for Electrical Engineering Technology students. *Proceedings of the International Symposium on Modern Electric Power Systems (MEPS '10)*, pp. 1–6, September 2010.
- [19] Lu R, Zhu C, Tian L, Wang Q. Super-capacitor stacks management system with dynamic equalization techniques. *IEEE Trans Magn.* 2020;43(1):254–8.
- [20] Gworcía P, Gworcía CA, Fernandez LM, Llorens F, Jurado F. ANFIS-based control of a grid-connected hybrid system integrating renewable energies, hydrogen and batteries. *IEEE Trans Ind Inf.* 2014;10:1107–17. doi: 10.1109/TII.2013.2290069.
- [21] GWorcía P, Torreglosa JP, Fernandez LM, Jurado F. Optimal energy management system for stand-alone wind turbine/photovoltaic/hydrogen/battery hybrid system with supervisory control based on fuzzy logic. *Int J Hydrog Energ.* 2013;38:14146–58. doi: 10.1016/j.ijhydene.2013.08.106.
- [22] Li J, Liu Y, Wang S, Shi J, Ren L, Gong K, et al. Design and advanced control strategies of a hybrid energy storage system for the grid integration of wind power generations. *IET Renew Power Gener.* 2015;9:89–98. doi: 10.1049/iet-rpg.2013.0340.
- [23] Sarvi M, Avanaki IN. An optimized fuzzy logic controller by water cycle algorithm for power management of stand-alone hybrid green power generation. *Energy Convers Manag.* 2015;106:118–26. doi: 10.1016/j.enconman.2015.09.021.
- [24] Yumurtaci R. Role of energy management in hybrid renewable energy systems: case study based analysis considering varying seasonal conditions. *Turk J Electr Eng Comput Sci.* 2013;21:1077–91. doi: 10.3906/elk-1112-85.
- [25] Dash P, Athari MH, Ardehali MM. Operational performance of energy storage as function of electricity prices for on-grid hybrid renewable energy system by optimized fuzzy logic controller. *Renew Energ.* 2016;85:890–902. doi: 10.1016/j.renene.2015.07.055.
- [26] Safari S, Ardehali MM, Sirizi MJ. Particle swarm optimization based fuzzy logic controller for autonomous green power energy system with hydrogen storage. *Energy Convers Manag.* 2013;65:41–9. doi: 10.1016/j.enconman.2012.08.012.
- [27] Cozzolino R, Tribioli L, Bella G. Power management of a hybrid renewable system for artificial islands: a case study. *Energ.* 2016;106:774–89. doi: 10.1016/j.energy.2015.12.118.
- [28] Dash V, Bajpai P. Power management control strategy for a stand-alone solar photovoltaic-fuel cell/battery hybrid system. *Sustain Energy Technol Assess.* 2015;9:68–80. doi: 10.1016/j.seta.2014.10.001.
- [29] Brka A, Kothapalli G, Al-Abdeli YM. Predictive power management strategies for stand-alone hydrogen systems: lab-scale validation. *Int J Hydrog Energ.* 2015;40:9907–16. doi: 10.1016/j.ijhydene.2015.06.081.
- [30] Akcayol MA. Application of adaptive neuro-fuzzy controller for SRM. *Adv Eng Softw.* 2004;35:129–37. doi: 10.1016/j.advengsoft.2004.03.005.
- [31] GWorcía-Torres F, Bordons C. Optimal economical schedule of hydrogen-based microgrids with hybrid storage using model predictive control. *IEEE Trans Ind Electron.* 2015;62:5195–207. doi: 10.1109/TIE.2015.2412524.
- [32] Kuperman A, Aharon I. Battery-ultracapacitor hybrids for pulsed current loads: a review. *Renew Sustain Energy Rev.* 2011;15:981–92. doi: 10.1016/j.rser.2010.11.010.
- [33] Zhang ZYZ, Jiang ZJZ, Yu XYX. Control strategies for battery/super-capacitor hybrid energy storage systems. *2008 IEEE Energy 2030 Conf*, pp. 5–10, 2008. doi: 10.1109/ENERGY.2008.4781031.
- [34] Mendis N, Muttaqi KM, Perera S. Active power management of a super capacitor-battery hybrid energy storage system for stand-alone operation of DFIG based wind turbines. *2012 IEEE Ind Appl Soc Annu Meet*, pp. 1–8, 2012. doi: 10.1109/IAS.2012.6374045.
- [35] Omar N, Mierlo JV, Verbrugge B, den Bossche PV. Power and life enhancement of battery-electrical double layer capacitor for hybrid electric and charge-depleting plug-in vehicle applications. *Electrochim Acta.* 2010;55:7524–31. doi: 10.1016/j.electacta.2010.03.039.
- [36] Lailier P, Zaninotto F, Nivet S, Torcheux L, Sarrau J-F, Vaurijoux J-P, et al. Study of the softening of the positive active-mass in valve-regulated lead-acid batteries for electric-vehicle applications. *J Power Sourc.* 1999;78:204–13. doi: 10.1016/S0378-7753(99)00038-5.
- [37] Ruetschi P. Aging mechanisms and service life of leadacid batteries. *J Power Sourc.* 2004;127:33–44. doi: 10.1016/j.jpowsour.2003.09.052.
- [38] Papazov G, Pavlov D. Influence of cycling current and power profiles on the cycle life of lead/acid batteries. *J Power Sourc.* 1996;62:193–9. doi: 10.1016/S0378-7753(96)02422-6.